High-Quality Fiber Bragg Grating Array for Quasi-Distributed High-Temperature Sensing

Xizhen Xu, Yonglan Zhang, Zhuoda Li, Zhiwei Qin, Runxiao Chen, Fan Zhou, Zhiyong Bai, Guo-Wei Lu, *Member, IEEE*, Yiping Wang, *Senior Member, IEEE*, and Jun He, *Member, IEEE*

***Abstract*—The wavelength-division-multiplexed (WDM) fiber Bragg grating (FBG) array inscribed by using femtosecond laser is a promising quasi-distributed temperature sensors due to its excellent thermal resistance. We developed the femtosecond laser point-by-point (PbP) inscription method to create the high-quality WDM FBG array featuring with uniform reflectivity, low polarization dependent loss (PDL), and high side-mode suppression ratio (SMSR). The shutter and the slit were inserted into the inscription system, which can be used to decrease the PDL and increase the uniformity in reflection of FBG. Moreover, the precise control over the position of refractive index modulations (RIMs) is used to realize apodized profiles, increasing the SMSR of FBG. By using these approaches, a high-quality WDM FBG array consisting of ten gratings was fabricated successfully. In addition, the FBG arrays packaged by stainless steel microtube were welded on the steel plate. High-temperature tests were carried out. The results show that the temperature distributions of the plate can be measured by using such WDM FBG arrays. Moreover, a 40-h, 700 °C test and a cycling temperatures test were performed. These arrays exhibited excellent high thermal stability and good repeatability in temperature measurements. Furthermore, a thermal shock test was carried out by using the flame projector, and the maximum temperature of 1000 °C was achieved. During the test, the sensors can measure the temperature stably. Hence, the proposed WDM FBG array is a promising quasi-distributed high-temperature sensor, which can be applied in many fields, for example, power plants, gas turbines, and hypersonic vehicles.**

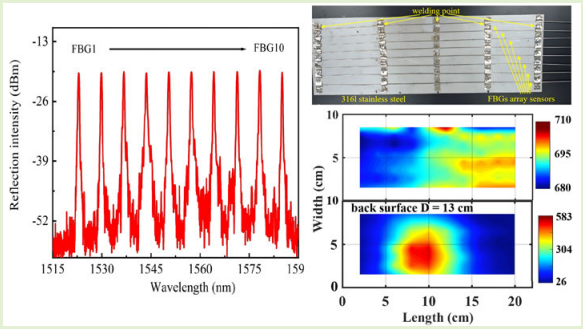

***Index Terms*— Femtosecond laser materials processing, high-temperature sensor, optical fiber Bragg grating (FBG).**

Received 5 November 2025; accepted 6 December 2025. Date of publication 22 December 2025; date of current version 2 February 2026. This work was supported in part by the National Key Research and Development Program of China under Grant 2023YFB3208600; in part by the National Natural Science Foundation of China (NSFC) under Grant 62435012, Grant 62375176, and Grant 62275169; in part by the Department of Science and Technology of Guangdong Province under Grant 2024TQ08Z673 and Grant 2024A1515010108; and in part by the Lingchuang Research Project of China National Nuclear Corporation under Grant CNNC LCKY-2024-067. The associate editor coordinating the review of this article and approving it for publication was Dr. Antreas Theodosiou. *(Corresponding author: Jun He.)*

Xizhen Xu, Yonglan Zhang, Zhuoda Li, Zhiwei Qin, Runxiao Chen, Zhiyong Bai, Yiping Wang, and Jun He are with the State Key Laboratory of Radio Frequency Heterogeneous Integration, Key Laboratory of Optoelectronic Devices and Systems, Ministry of Education/Guangdong Province, College of Physics and Optoelectronic Engineering, Shenzhen University, Shenzhen 518060, China, and also with Shenzhen Key Laboratory of Photonic Devices and Sensing Systems for Internet of Things, Guangdong and Hong Kong Joint Research Centre for Optical Fibre Sensors, Shenzhen University, Shenzhen 518060, China (e-mail: xizhenxu@szu.edu.cn; 2300453062@email.szu.edu.cn; 2100453028@email.szu.edu.cn; 2453232014@mails.szu.edu.cn; 2060453041@email.szu.edu.cn; baizhiyong@szu.edu.cn; ypwang@szu.edu.cn; hejun07@szu.edu.cn).

Fan Zhou is with the Innovation and Research Institute, HIWING Technology Academy, Beijing 100074, China (e-mail: 617754462@qq.com).

Guo-Wei Lu is with the Institute for Materials Chemistry and Engineering, Kyushu University, Fukuoka 816-8580, Japan (e-mail: gordon.guoweilu@gmail.com).

Digital Object Identifier 10.1109/JSEN.2025.3644178

I. Introduction

DISTRIBUTED high-temperature sensing (DTS) is significant in various application fields, such as metallurgy, aviation, and power plants [1], [2], [3], [4]. For example, when hypersonic vehicles travel at high speeds, its temperature would rise rapidly due to the aerodynamic heating. The surface of aircraft would suffer the large thermal loading, posing a threat to the structural safety [4]. This calls the distributed temperature monitoring on the thermal resistance materials. Thermocouples are typical high-temperature sensors, but they are single-point sensors, which are not suitable for distributed sensing. Temperature-sensitive paint and infrared thermal imagers can be employed to solve this issue. However, these two methods struggle to accurately measure and record the surface temperature of a high-speed flying aircraft.

DTS based on optical fibers is more attractive due to its compact size, capability of multiplexing, and immunity to electromagnetic interference. Raman- or Brillouin-based methods have been proposed to achieve distributed temperature monitoring, but these methods have a low spatial resolution (on the order of 1 m), which are merely suitable for measuring the temperature in a long sensing range (more than tens of kilometers) [5], [6]. The Rayleigh-based or the ultraweak fiber

Bragg grating (UWFBG)-based with optical frequency-domain reflectometer (OFDR) demodulation exhibits a higher spatial resolution (on the order of millimeters) [7], [8], [9]. However, such an OFDR system is expensive.

To achieve the distributed temperature monitoring with high spatial resolution and short sensing range, the wavelength-division-multiplexed (WDM) FBG array demodulated with multichannel FBG interrogator is a more promising method, due to its better cost-effectiveness. Such a system can realize a quasi-distributed temperature sensing with tens or hundreds measuring points [10], [11], [12]. Note that Mihailov et al. [13] reported the fabrication of FBGs by using femtosecond laser. It has been found that these FBGs can withstand temperatures of up to 1000 °C [14], [15], and then, the emergence of the point-by-point (PbP) inscription method has efficiently enhanced the preparation capacity of WDM FBG array [16]. The sensing performance depends on the spectral characteristics of FBG. Hence, researchers have made significant efforts to develop the PbP method to fabricate high-quality FBG [17], [18], [19], [20]. For example, the slit beam shaping method was proposed to decrease the polarization dependent loss (PDL) of FBG [17], [18], [19]. The precise control over the position of PbP refractive index modulations (RIMs) is used to create apodized FBG, enhancing the high side-mode suppression ratio (SMSR) [20]. In addition, Ioannou and Kalli [21] proposed the plane-by-plane method to create apodized FBGs with an impressive SMSR of 31.5 dB. These results demonstrate that SMSR and PDL have been optimized sufficiently, benefiting for improving precise and stability of sensing. However, the PbP WDM FBG array still has a main problem, i.e., the low uniformity of each reflection peak, which increases the difficulty in demodulation or even makes it impossible to identify the reflection peaks [19], [22]. This phenomenon mainly results from the insertion loss of each grating and the deviation between the PbP RIM and the core center (i.e., fluctuation in reflectivity). Therefore, it is necessary to propose an efficient method for preparing the high-quality WDM FBG array.

In this study, we developed the high-quality WDM FBG array created by using femtosecond laser PbP inscription method. Such a WDM FBG array features with uniform reflectivity, low PDL, and high SMSR. The slit beam shaping method is employed to reduce the birefringence of FBG, decreasing the PDL of array. The precise control over the position of PbP RIMs is used to achieve apodized profiles, increasing the SMSR of array. The shutter controlled by the FBG interrogator can be employed to create the WDM array with uniform reflection. A high-quality WDM FBG array consisting of ten gratings can be achieved by using the above-mentioned methods. Moreover, eight arrays were packaged by stainless steel micro tube, serving as high-temperature sensors, which were fixed on a stainless-steel plate by means of welding. High-temperature tests by using the furnace and the flame projector were carried out. The temperature distributions of the plate can be measured. These results show that such a WDM FBG array is suitable for quasi-DTS in a short range.

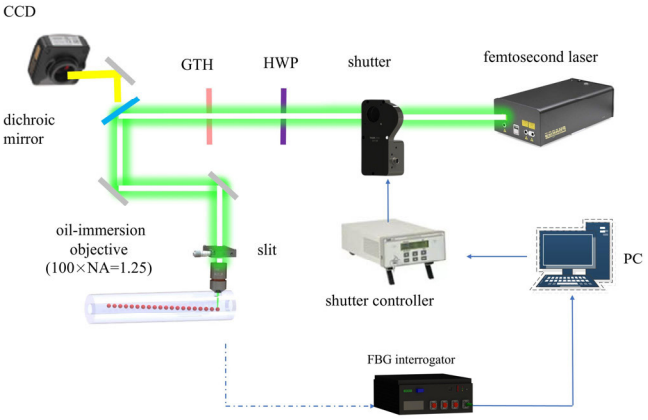

Fig. 1. Schematic of the high-quality WDM FBG array by using femtosecond laser point-by-point technique. HWP, half-wave plate; GP, Glan-Thompson prism; CCD, charge coupled device; and PC, personal computer.

II. Device Fabrication and Characterization

The principle and experimental setup used for fabricating high-quality WDM FBG array by using femtosecond laser PbP technology were exhibited in Fig. 1. A femtosecond laser with a central wavelength of 515 nm, a pulsewidth of 245 fs, a repetition rate of 1 kHz, and a laser spot diameter of 3 mm was employed as the laser source. The pulse energy was adjusted using a half-wave plate (HWP) and a Glan-Thompson prism (GP). A 100× Leica oil-immersion objective with a numerical aperture (N.A.) of 1.25 served as the focusing element. Note that the index-matching oil was applied to eliminate the distortion to the focus of the laser induced by the cylindrical geometry of the fiber. An adjustable mechanical slit (Thorlabs, VA100) was inserted in front of the objective. The slit position and inclination were set to ensure the normal incidence of beam center, and the slit orientation was set to parallel to the fiber axis. The circular cross-sectional patterns of RIM can be achieved, leading to low birefringence and low PDL of PbP FBG. Moreover, the shutter controlled by FBG interrogator (MOI Si255) was inserted in front of the output of the femtosecond laser. The reflection spectrum of FBG is measured by the interrogator. This device has a wavelength range of 1510–1590 nm, i.e., the bandwidth of 80 nm. The wavelength demodulation accuracy and the demodulation speed are 2 pm and 5 kHz, respectively. During the inscription process, when the reflectivity achieves the set value, the shutter is closed immediately. The laser beam is cut off. By using this method, the reflectivity of each grating can be consistent. The single-mode fibers (SMFs, Corning SMF-28e) were moved precisely using a 3-D air-bearing translation stage (Aus-precision, QFL-100XY for the x- and y-axes and RBN-Z-5 for the z-axis). The period of FBG depends on the repetition rate and the velocity of translation stage. It is flexible to fabricate WDM FBG array. Moreover, the apodized modulation profiles can be realized precisely via control over the transverse position of each laser-inscribed RIM, as shown in Fig. 1, improving the SMSR of FBG.

At first, we investigated the effect of the use of the slit on the PDL of the FBG. A PbP FBG S1 was inscribed without slit,

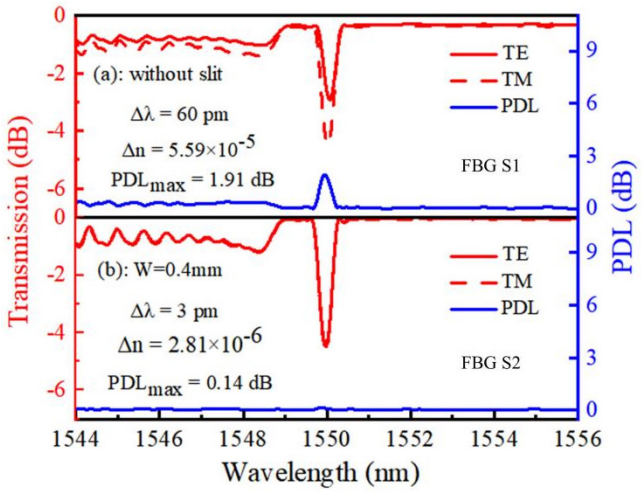

Fig. 2. Corresponding transmission spectra of two orthogonal linear polarization modes (TE and TM) and PDL spectra. (a) FBG S1 inscribed without slit beam shaping and (b) FBG S2 inscribed using slit beam shaping with a slit width of 2 mm.

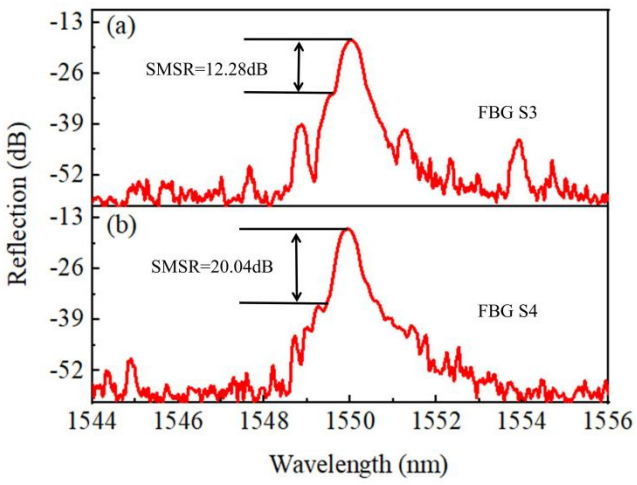

Fig. 3. Reflection spectra of (a) uniform FBG S3 and (b) Gaussian-apodized FBG S4.

TABLE I
PARAMETER COMPARISON OF WDM FBGS ARRAY (FBG1–FBG10)

Samples	Wavelength/ nm	Reflection/dBm	3-dB bandwidth/nm	SMSR/dB
FBG1	1522.90	-19.93	0.40	19.33
FBG2	1529.90	-19.95	0.42	19.97
FBG3	1536.80	-19.73	0.46	15.41
FBG4	1543.58	-19.93	0.40	16.21
FBG5	1550.38	-19.87	0.44	18.90
FBG6	1557.42	-19.64	0.42	15.46
FBG7	1564.18	-19.81	0.45	15.08
FBG8	1571.40	-19.61	0.42	17.85
FBG9	1578.12	-19.65	0.45	19.69
FBG10	1585.08	-19.93	0.40	19.95

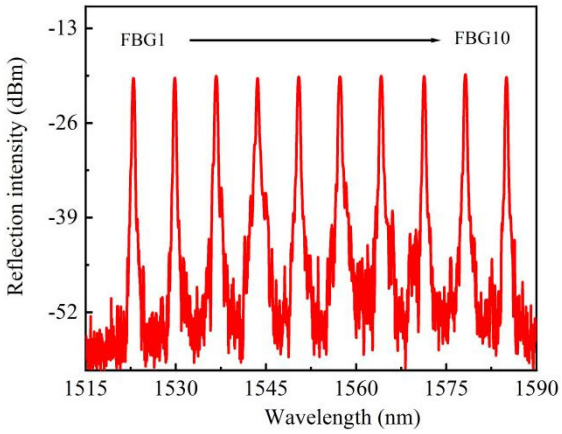

Fig. 4. Corresponding reflection spectrum of WDM FBG array including ten FBGs.

and a PbP FBG S2 was inscribed by using the slit with a width of 2 mm. Note that two FBGs have the same grating pitch of 1.070 μm and the same grating length of 2 mm. The on-target pulse energy of 39 nJ was used to create these two samples. The corresponding polarization-resolved transmission spectra and PDL spectra were measured by using a Muller-matrix-based commercial polarization analysis system, consisting of a tunable laser (Keysight, 81940A), a polarization synthesizer (Keysight, N7786B), and an optical power meter (Keysight, N7744A). As shown in Fig. 2(a) and (b), these two FBGs have the same Bragg wavelength of 1550 nm, similar dip attenuation of about −4 dB. Note that the difference between the Bragg wavelength of dip, and the birefringence, and the maximum of PDL of S2 are 3 pm, 2.81 $\times$ 10^{-6}, and 0.14 dB, which are much lower than that of S1 (i.e., 60 pm, 5.59 $\times$ 10^{-5}, and 1.91 dB). This result demonstrates that the PDL can be reduced efficiently since the RIM with circular cross-sectional pattern can be achieved by using slit beam shaping method [15].

Subsequently, we fabricated two FBGs (i.e., S3 and S4) by using femtosecond laser PbP technology, and these samples have the same grating pitch of 1.070 μm and the same grating length of 2 mm. Note that S3 is a nominal PbP FBG, and S4 is an apodized FBG, in which the offset of the RIM from the center of the core varies as Gaussian functions of the position of the fiber axis. As shown in Fig. 3(a) and (b), the reflection spectra of S4 exhibit the SMSR of 20.04 dB, which is higher than that of S3 (i.e., 13.28 dB). As a result, by using slit beam shaping method and the apodized method, the high-quality reflection spectrum of PbP FBG can be realized, which is beneficial to enhance the precise and stability in wavelength demodulation.

Moreover, we fabricated WDM FBG arrays consisting of ten FBGs (i.e., FBG1-FBG10) by using the slit beam shaping method and the Gaussian-apodized approach. The distance between adjacent gratings is 2 cm, and the on-target single pulse energy used for fabricating these FBGs was 39 nJ. All of them are type II gratings. The reflection intensity of each FBG was controlled by the shutter. As shown in Fig. 4, the reflection spectrum of array exhibits uniform intensity and high SMSR. As displayed in Table I, the Bragg wavelength of these FBGs is ranging from 1522 to 1585 nm. The 3-dB bandwidth and the reflection intensity are about ∼0.40 nm and −21 dBm, respectively. Note that the difference in reflection intensity is less than 0.34 dB.

Subsequently, torsion and vibration are two most widespread external perturbations in application environments, which would hamper the stability of spectrum of FBG. Hence, we further evaluated the effect of torsion and vibration on

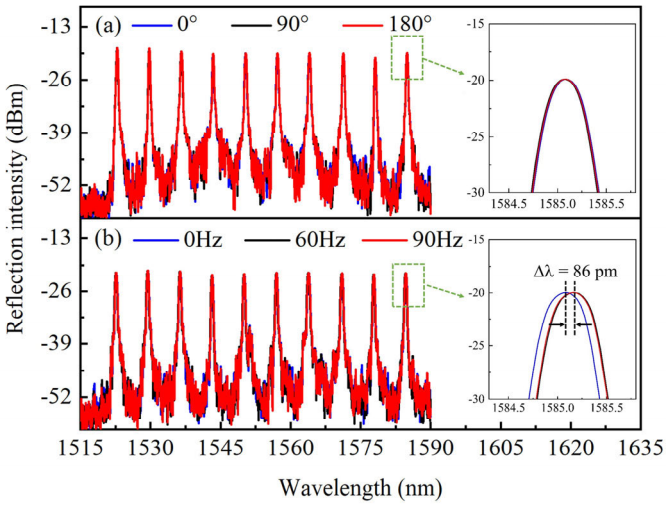

Fig. 5. Reflection spectra of the WDM FBG array (a) twisted with a range of 0°–180° or (b) vibrated with a frequency range of 0–90 Hz and a random acceleration of 1–13 g.

the stability of the WDM FBG array. At first, the array was twisted in a range of 0°–180°. As shown in Fig. 5(a), compared with the blue curve (i.e., fiber without twisting), the black curve (i.e., fiber twisted by 90°) and the red curve (i.e., fiber twisted by 180°) exhibit no obvious change in the intensity of the peak or the shift in the Bragg wavelength. Some fluctuations in the intensity of the bottom of spectrum can be observed, which has no effect on the SMSR of FBG. The reflection peak of FBG10 was zoomed in and shown in the inset of Fig. 5(a). Three curves were completely overlapping. This means that the spectrum exhibits excellent stability when the FBG array was twisted with various angles. This benefits from the low PDL of array. In addition, the vibration test was carried out by employing the system consisting of a signal generator, charge amplifier, accelerometer, vibration stage, and oscilloscope. The array was fixed to the vibration stage. The range of vibration frequency was set as 0–90 Hz. The vibration acceleration was varied randomly ranging from 1 to 13 g ($g \approx 9.8$ m/s^2). As shown in Fig. 5(b), the intensity of these reflection peaks at various vibration frequencies (i.e., 60 and 90 Hz) exhibits no obvious change. The fluctuations merely exist at the bottom of spectrum, but the reflection peak has a red shift of 86 pm, as displayed in the inset of Fig. 5(b). The reason for this phenomenon is that the FBG fixed on the stage would be stretched slightly when it is subjected to vibration. This problem can be solved by using a stress-free packaging structure.

III. High-Temperature Characteristics

The bare WDM FBG array is fragile in actual environment. A 316l stainless steel tube can suffer 800 °C for long term and even temporarily endure temperatures of up to 1200 °C. Moreover, this tube exhibits high ductility for easy installation, while it maintains high mechanical strength, ensuring reliable protection, and hence, we used this tube with a diameter of 0.8 mm to package array, serving as quasi-distributed temperature sensors. Note that the FBG array was not connected to the inner surface of the tube by using adhesive or welding, eliminating the influence of external stress. To improve the stability of the sensors, the annealing process at 800 °C for 30 h was implemented, and then, the temperature response was tested by placing the arrays into a tube furnace (Panran, Gero EST12/300). In order to achieve accurate in situ temperature measurement, ten K-type thermocouples were placed along each FBG to record the temperature as a reference. The accuracy of such a thermometer is $\pm 0.25\%T$, where T is the measured temperature. The temperature in the furnace varied from 20 °C to 700 °C and was maintained for 30 min at each measurement point. During the calibration process, we recorded the Bragg wavelength of array and corresponding temperature. The complete high-temperature response of the FBG array is displayed in Fig. 6(a). The temperature sensitivity of FBG can be expressed as $\Delta\lambda_B/\Delta T = \lambda_B(\alpha + \xi)$, where λ_B is the Bragg wavelength and α and ξ are the thermal expansion coefficient and the thermal optical coefficient of the fiber material, respectively [23]. The temperature sensitivity of FBG is not the constant. When the temperature increases, the Bragg wavelength exhibits a red shift and the slope increases. Hence, a third-order polynomial curve: $\lambda_B = A + B \times T + C \times T^2 + D \times T^3$ was employed to evaluate the temperature response. Note that the fit curve of FBG10 only reached 400 °C, since the reflection peak of FBG10 shifted out of the wavelength range of the interrogator. The curve with high fitness ($R^2 = 0.999$) was realized. The fitting parameters (i.e., A–D) of the various curves of the FBG array are demonstrated in Table II. For each FBG with the same Bragg wavelength in the different array, we use the same fitting curve. As shown in Fig. 6(b), ten arrays, including 80 FBGs, exhibit the slightly large temperature uncertainty of ±5 °C. This results mainly from the dispersion of the Bragg wavelength, even if the same fabrication parameters are used. The temperature uncertainty can be reduced, when each FBG has its own dedicated fitting curve. However, this method would hinder the widespread adoption of FBG sensors. The fundamental solution to this problem lies in overcoming the challenge of improving Bragg wavelength consistency during the fabrication process of FBG.

Here, we employed the eight packaged FBG arrays to measure the temperature distribution of the 316l steel plate with a width of 10 cm and a length of 20 cm. Eight FBG arrays can serve as 80 measuring points [i.e., red circular plotted in Fig. 7(a)]. The layout of the FBG sensors on the

TABLE II
Fitting Coefficients of the FBG Array Sensor Using a Cubic Function

Samples	A	B	C	D
FBG1	1522.33037	0.00914	1.02831E-5	-5.43135E-9
FBG2	1529.34861	0.0091	1.04212E-5	-5.50288E-9
FBG3	1536.19707	0.00886	1.08946E-5	-5.79913E-9
FBG4	1543.0134	0.00894	1.07476E-5	-5.62277E-9
FBG5	1549.92465	0.00918	1.0404E-5	-5.30286E-9
FBG6	1556.79066	0.00941	1.00056E-5	-5.03941E-9
FBG7	1563.56635	0.00906	1.05396E-5	-5.2458E-9
FBG8	1570.67325	0.00913	1.07166E-5	-5.46691E-9
FBG9	1577.48539	0.00872	1.11107E-5	-5.25185E-9
FBG10	1584.21931	0.00854	1.35565E-5	-8.89633E-9

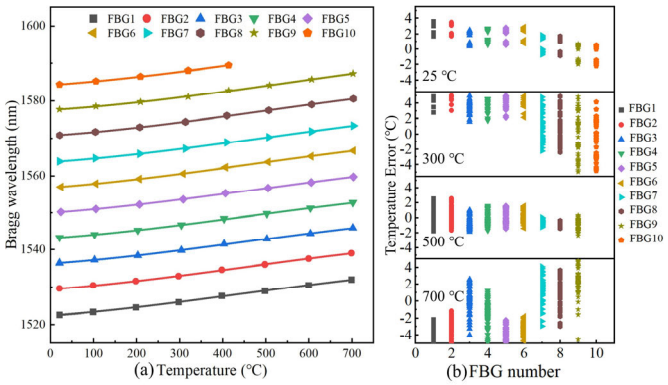

Fig. 6. Study of temperature calibration of the WDM FBG array at elevated temperatures ranging from room temperature to 700 °C. (a) Temperature response with polynomial fit curves of ten FBGs. (b) Temperature error of ten FBGs at 25 °C, 300 °C, 500 °C, and 700 °C.

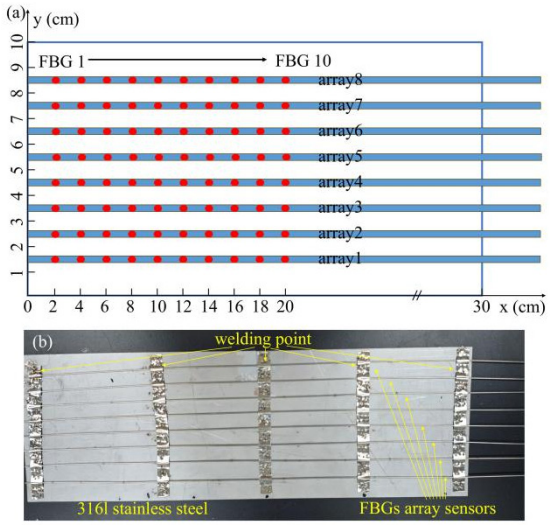

Fig. 7. (a) Schematic and (b) image of the 316l plate with eight packaged WDM FBG array sensors fixed on the surface.

front plate of the 316l plate is shown in Fig. 7(b). By covering a slender 316l steel onto the sensor and welding it to the plate, the sensor can be attached to the plate. The slender with the width of 8 mm was placed between two adjacent gratings, but it did not cover the gratings. This method can prevent the sensors from being damaged by the welding process. Moreover, the tight connection ensures that the heat of the plate is quickly transferred to the sensor, thereby improving the response speed. The interrogator (MOI Si255) and the 1 × 8 optical switch module were employed for demodulation of eight FBG arrays.

The 316l plate was placed in the Muffle furnace. Temperature varies from room temperature to 700 °C. By using the fitting curves of sensors, temperatures of eighty measurement points can be obtained. The 2-D interpolation algorithm was employed to compute the temperature gradients, and the contour points were taken into account for boundary conditions at this algorithm. Then, by using the temperature data measured by FBGs, the temperature distribution of the plate can be achieved. When the plate was placed at various temperatures of 26 °C, 350 °C, 550 °C, and 700 °C, the temperature distributions represented by a relative colormap were shown in

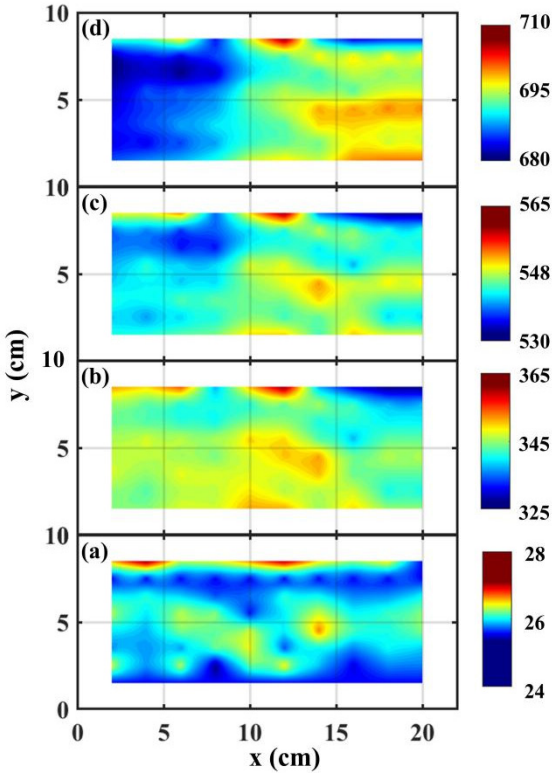

Fig. 8. Temperature distribution of the 316l steel plate. Maximum temperatures of around (a) 26 °C, (b) 350 °C, (c) 550 °C, and (d) 700 °C.

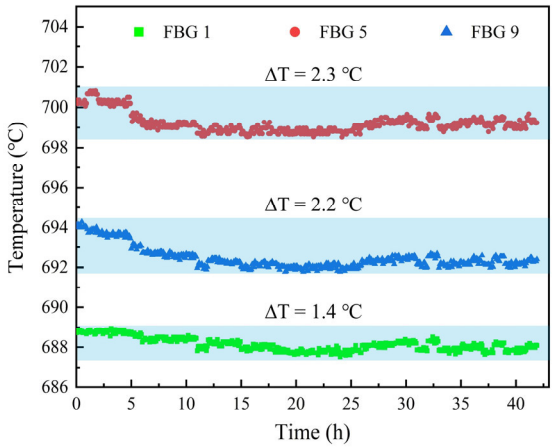

Fig. 9. Stability of the FBG1, FBG5, and FBG9 of array5 at a temperature above 700 °C over 40 h.

Fig. 8(a)–(d). In case of 26 °C, the maximum of temperature different is merely 4 °C, resulting from the measurement error of the FBG sensors. When the furnace temperature increases to 350 °C, the maximum of temperature difference exhibits a significant increase (i.e., ∼40 °C). This reason for this phenomenon is that the heating zone of the furnace is not uniformity. When the temperature further increases to 550 °C and 700 °C, the different of temperature distribution exhibits a decrease of 35 °C and 30 °C, respectively, resulting from the more uniform temperature field of the furnace at high temperatures of up to 500 °C. These results demonstrated that the proposed WDM FBG array is fully capable of measuring the temperature distribution of a plate.

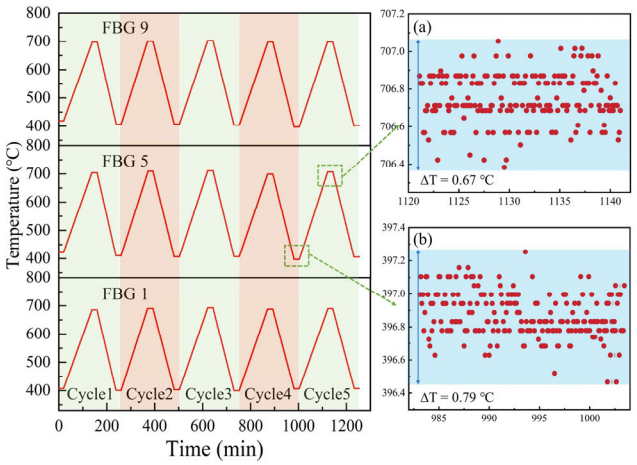

Fig. 10. Cycling temperatures test between 400 °C and 700 °C of FBG1, FBG5, and FBG9 of array5. (Insets) Temperature fluctuations recorded by FBG5 at (a) 700 °C and (b) 400 °C.

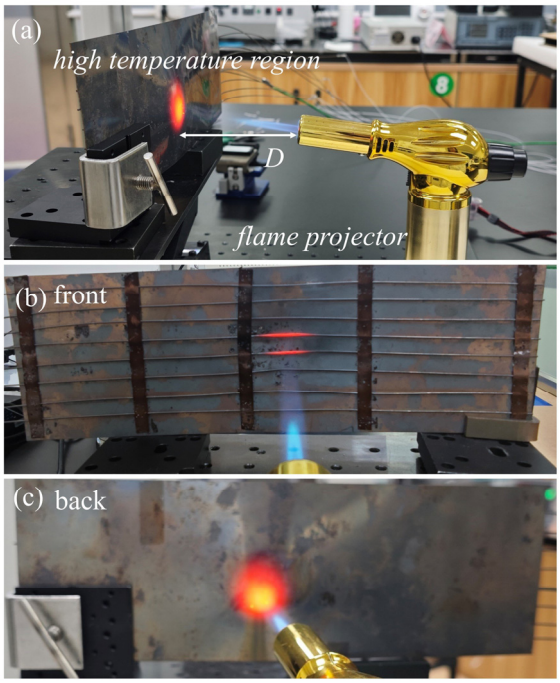

Fig. 11. (a) 316l plate with eight packaged WDM FBG array sensors fixed on the surface was heated by using the flame projector. Images of (b) front surface and (c) back surface of the plate burned by the flame.

A 40-h, 700 °C stability test was carried out by using the 316l plate with FBG array. The evolutions of temperature measured by FBG1, FBG5, and FBG9 of array5 were shown in Fig. 9. The means of temperatures measured by these FBGs are 698 °C, 693 °C, and 688 °C, respectively. The deviations of the measured temperatures are 1.4 °C, 2.2 °C, and 2.3 °C, resulting from the fluctuations in temperature field of muffle furnace. Hence, the proposed FBG array exhibits an excellent long-term high thermal stability. Moreover, the repeatability of FBG array was investigated via cycling temperatures test. At first, the temperature increased to 700 °C and was maintained for 20 min, and then, it decreased to 400 °C. Five cycles were performed. The temperatures recorded by FBG1, FBG5, and FBG9 of array5 have been displayed in Fig. 10. To further

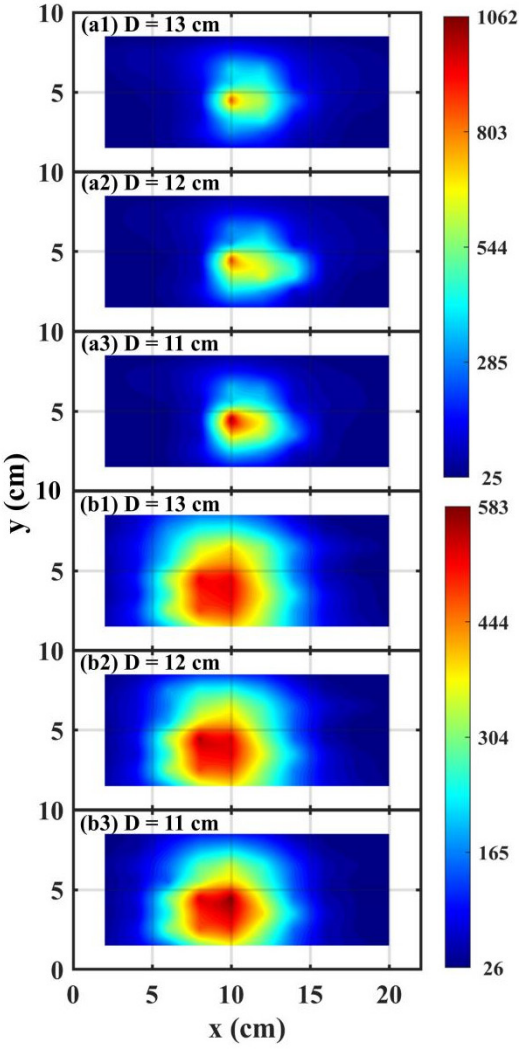

Fig. 12. Temperature distribution of the plate was measured by using eight FBG arrays when the flame burns (a1)–(a3) front surface and (b1)–(b3) back surface of the plate by using the flame projector. Distances between the pate and the projector were set as 11, 12, and 13 cm, respectively.

observe the detail of the temperature curve, the fifth cycle recorded by FBG5 of array5 is zoomed in, as shown in the insets (a) and (b) of Fig. 10. The fluctuations in temperature at high temperature point (i.e., 700 °C) and low temperature point (i.e., 400 °C) is 0.67 °C and 0.79 °C, respectively. These experimental results demonstrate that these FBGs have the good repeatability in temperature measurements.

Moreover, the 316l plate was heated by using the flame projector, as shown in Fig. 11(a). The local high-temperature region can be achieved. At first, the flame burns the front surface of the plate, where the sensor is installed, as displayed in Fig. 11(b). The projector was placed at varying distances (i.e., 11, 12, and 13 cm) from the plate. As shown in Fig. 12(a1)–(a3), the maximum temperature exceeds 1050 °C, and the maximum temperature gradient is up to 200 °C/cm in these three colormaps, and the red region (i.e., its temperature of up to 800 °C) exhibits obviously expansion with decreasing distance of 13, 12, and 11 cm. This is because more heat is transferred to the plate and the sensors, when the projector

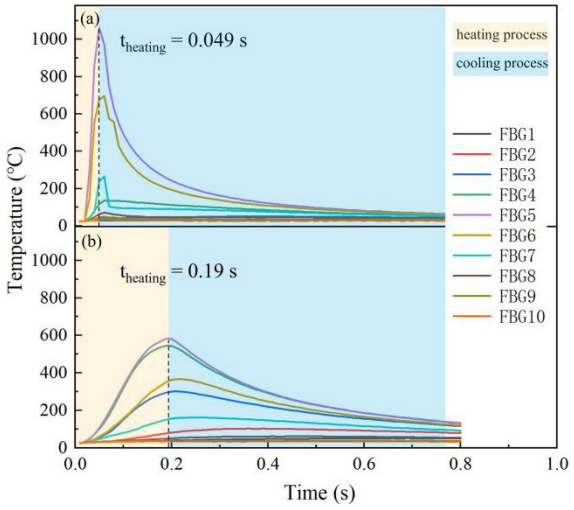

Fig. 13. Evolution of temperature was measured by the WDM FBG array4, when (a) front surface and (b) back surface of the plate were heated by using the flame projector. Distance between the projector and the plate was set as 11 cm.

approaches the plate. Notably, in the heating process, the temperature increased quickly, as shown in Fig. 13(a). The temperature rises from room temperature to 1061 °C measured by the FBG5 sensor of array4, which costs only 0.049 s, and then, the projector was closed, the temperature dropped. The heating and cooling process was completely recorded. These results demonstrate that the proposed FBG array sensors can suffer the thermal shock and measure temperature stably.

However, when the flame burns the front surface of the plate (i.e., the surface installed with the sensors), both the sensors and the plate were heated simultaneously by the flame. In other words, the temperature of the flame and the plate was measured by the sensors. Then, the temperature distribution of the plate cannot be measured precisely. As displayed in Fig. 11(c), the flame burns the back surface of the plate with decreasing distance (13, 12, and 11 cm). As illustrated in Fig. 12(b1)–(b3), the temperature regions exhibit "smoother." The maximum temperature and the gradient have shown a significant decrease (i.e., 550 °C and 88 °C /cm), which are half of the values demonstrated in Fig. 12(a1)–(a3). This results from that the sensors will be heated slowly when the flame burns the back surface of the plate. As shown in Fig. 13(b), the heating process costs 0.19 s, which is indeed slower than that observed in Fig. 13(a). In this test, without interference from the flame, the temperature distribution of the 316l plate can be measured precisely.

IV. Conclusion

In this work, we have reported on the high-quality WDM FBG array inscribed by using femtosecond laser PbP inscription method for quasi-distributed temperature sensing. Such a WDM FBG array, featuring with uniform reflectivity (i.e., difference of less than 0.34 dB), low PDL of 0.14 dB, and high SMSR of more than 15 dB, was fabricated with the shutter, the slit, and the precise control over the position of RIMs. Moreover, these FBG arrays packaged by stainless steel microtube serve as high-temperature sensors, which were welded on the 316l steel plate. High-temperature tests were carried out by using the furnace and the flame projector. The experimental results show that such FBG arrays with excellent long-term high thermal stability and good repeatability in temperature measurements can be employed for measuring the temperature distribution of plate. Moreover, it can survive and work stably in rapid heating processes, such as a 1000 °C temperature spike in just 0.049 s. Therefore, the packaged WDM FBG array is a promising sensor, which can be used for quasi-distributed high-temperature measurement in various fields, such as power plants, gas turbines, and hypersonic vehicles.

References

[1] A. Kus, Y. Isik, M. Cakir, S. Coşkun, and K. Özdemir, "Thermocouple and infrared sensor-based measurement of temperature distribution in metal cutting," *Sensors*, vol. 15, no. 1, pp. 1274–1291, Jan. 2015.

[2] G. Laffont, R. Cotillard, N. Roussel, R. Desmarchelier, and S. Rougeault, "Temperature resistant fiber Bragg gratings for on-line and structural health monitoring of the next-generation of nuclear reactors," *Sensors*, vol. 18, no. 6, p. 1791, Jun. 2018.

[3] W. Yan, Y. Ya, F. Du, H. Shao, and P. Zhao, "Spectrometer-based line-of-sight temperature measurements during alkali-pulverized coal combustion in a power station boiler," *Energies*, vol. 10, no. 9, p. 1375, Sep. 2017.

[4] R. J. Black, J. M. Costa, L. Zarnescu, D. A. Hackney, B. Moslehi, and K. J. Peters, "Fiber-optic temperature profiling for thermal protection system heat shields," *Opt. Eng.*, vol. 55, no. 11, Oct. 2016, Art. no. 114101.

[5] M. A. Soto et al., "Raman-based distributed temperature sensor with 1 m spatial resolution over 26 km SMF using low-repetition-rate cyclic pulse coding," *Opt. Lett.*, vol. 36, pp. 2557–2559, Jul. 2011.

[6] F. Wang, C. Zhu, C. Cao, and X. Zhang, "Enhancing the performance of BOTDR based on the combination of FFT technique and complementary coding," *Opt. Exp.*, vol. 25, no. 4, pp. 3504–3513, 2017.

[7] M. Luo, J. Liu, C. Tang, X. Wang, T. Lan, and B. Kan, "0.5 mm spatial resolution distributed fiber temperature and strain sensor with position-deviation compensation based on OFDR," *Opt. Exp.*, vol. 27, pp. 35823–35829, Nov. 2019.

[8] B. Xu et al., "Femtosecond laser point-by-point inscription of an ultra-weak fiber Bragg grating array for distributed high-temperature sensing," *Opt. Exp.*, vol. 29, no. 20, pp. 32615–32626, 2021.

[9] B. Du et al., "Femtosecond laser-induced in-fiber composite microcavity array for high-performance distributed high-temperature sensing," *IEEE Trans. Instrum. Meas.*, vol. 73, pp. 1–9, 2024.

[10] Y. Ou et al., "Large WDM FBG sensor network based on frequency-shifted interferometry," *IEEE Photon. Technol. Lett.*, vol. 29, no. 6, pp. 535–538, Mar. 15, 2017.

[11] C.-H. Yeh, Y.-H. Zhuang, N. Tsai, and C.-W. Chow, "Capacity and capability enhancements of FBG sensor system by utilizing intensity and WDM detection technique," *Smart Mater. Struct.*, vol. 26, no. 3, Mar. 2017, Art. no. 035026.

[12] R. Rodríguez-Garrido et al., "High-temperature monitoring in central receiver concentrating solar power plants with femtosecond-laser inscribed FBG," *Sensors*, vol. 21, no. 11, p. 3762, May 2021.

[13] S. J. Mihailov et al., "Fiber Bragg gratings made with a phase mask and 800-nm femtosecond radiation," *Opt. Lett.*, vol. 28, no. 12, pp. 995–997, 2003.

[14] D. Grobnic, C. W. Smelser, S. J. Mihailov, and R. B. Walker, "Long-term thermal stability tests at 1000 °C of silica fibre Bragg gratings made with ultrafast laser radiation," *Meas. Sci. Technol.*, vol. 17, no. 5, pp. 1009–1013, May 2006.

[15] H. Chikh-Bled, K. Chah, Á. González-Vila, B. Lasri, and C. Caucheteur, "Behavior of femtosecond laser-induced eccentric fiber Bragg gratings at very high temperatures," *Opt. Lett.*, vol. 41, no. 17, pp. 4048–4051, 2016.

[16] A. Martinez, M. Dubov, I. Khrushchev, and I. Bennion, "Direct writing of fibre Bragg gratings by femtosecond laser," *Electron. Lett.*, vol. 40, no. 19, pp. 1170–1172, Sep. 2004.

[17] X. Xu et al., "Slit beam shaping for femtosecond laser point-by-point inscription of high-quality fiber Bragg gratings," *J. Lightw. Technol.*, vol. 39, no. 15, pp. 5142–5148, Aug. 15, 2021.

[18] P. Roldán-Varona, D. Pallarés-Aldeiturriaga, L. Rodríguez-Cobo, and J. M. López-Higuera, "Slit beam shaping technique for femtosecond laser inscription of enhanced plane-by-plane FBGs," *J. Lightw. Technol.*, vol. 38, no. 16, pp. 4526–4532, Aug. 15, 2020.
[19] R. Chen, J. He, X. Xu, J. Wu, Y. Wang, and Y. Wang, "High-quality fiber Bragg gratings inscribed by femtosecond laser point-by-point technology," *Micromachines*, vol. 13, no. 11, p. 1808, Oct. 2022.
[20] R. J. Williams et al., "Point-by-point inscription of apodized fiber Bragg gratings," *Opt. Lett.*, vol. 36, no. 15, pp. 2988–2990, 2011.
[21] A. Ioannou and K. Kalli, "Femtosecond laser inscribed fiber Bragg gratings based on precise spatial apodization," *Opt. Lett.*, vol. 48, no. 7, pp. 1826–1829, 2023.
[22] X. Liu et al., "Low short-wavelength loss fiber Bragg gratings inscribed in a small-core fiber by femtosecond laser point-by-point technology," *Opt. Lett.*, vol. 44, no. 21, pp. 5121–5124, 2019.
[23] A. D. Kersey et al., "Fiber grating sensors," *J. Lightw. Technol.*, vol. 15, no. 8, pp. 1442–1463, Aug. 15, 1997.

Xizhen Xu was born in Guangdong, China, in 1990. He received the B.S. degree from the College of Science, Zhejiang University of Technology, Hangzhou, China, in 2013, and the M.S. and Ph.D. degrees in optical engineering from Shenzhen University, Shenzhen, China, in 2016 and 2019, respectively.

From 2019 to 2021, he was a Postdoctoral Research Fellow with Shenzhen University, where he is currently an Assistant Professor. He has authored or co-authored six patent applications and more than 70 journal articles and conference papers. His research interests include femtosecond laser micromachining, optical fiber sensors, and fiber Bragg gratings.

Yonglan Zhang was born in Guangdong, China, in 2000. She received the B.S. degree in light sources and lighting from Jiaying University, Meizhou, China, in 2023. She is currently pursuing the M.S. degree with Shenzhen University, Shenzhen, China.

Her current research interests include optical fiber sensors and temperature field distributions.

Zhuoda Li was born in Inner Mongolia, China, in 1998. He received the B.Eng. degree from the College of Physics and Optoelectronic Engineering, Shenzhen University, Shenzhen, China, in 2021, where he is currently pursuing the Ph.D. degree in optical engineering.

His current research interests include optical fiber sensors and fiber Bragg gratings.

Zhiwei Qin was born in Hunan, China, in 1998. He received the B.Eng. degree from the School of Resources, Environment and Safety Engineering, University of South China, Hengyang, China, in 2021. He is currently pursuing the Ph.D. degree in optical engineering with Shenzhen University, Shenzhen, China.

His current research interests include fiber-optic smart sensing technologies.

Runxiao Chen was born in Guangdong, China, in 1998. He received the B.S. degree from the College of Physics and Optoelectronic Engineering, Shenzhen University, Shenzhen, China, in 2020, where he is pursuing the Ph.D. degree.

His current research interests focus on femtosecond laser micromachining, fiber lasers, and optical fiber sensors.

Fan Zhou, photograph and biography not available at the time of publication.

Zhiyong Bai was born in Henan, China, in 1984. He received the Ph.D. degree in optics from Nankai University, Tianjin, China, in 2014.

Since 2015, he has been with Shenzhen University, Shenzhen, China, as a Postdoctoral Research Fellow. Since 2018, he has been with Shenzhen University, as an Assistant Professor. His research interests include optical fiber gratings and orbital angular momentum.

Guo-Wei Lu (Member, IEEE), photograph and biography not available at the time of publication.

Yiping Wang (Senior Member, IEEE) was born in Chongqing, China, in 1971. He received the B.Eng. degree in precision instrument engineering from Xi'an Institute of Technology, Xi'an, China, in 1995, and the M.S. and Ph.D. degrees in optical engineering from Chongqing University, Chongqing, in 2000 and 2003, respectively.

From 2003 to 2005, he was with Shanghai Jiao Tong University, China, as a Postdoctoral Fellow. From 2005 to 2007, he was with Hong Kong Polytechnic University, Hong Kong, as a Postdoctoral Fellow. From 2007 to 2009, he was with the Institute of Photonic Technology (IPHT), Jena, Germany, as a Humboldt Research Fellow. From 2009 to 2011, he was with the Optoelectronics Research Centre (ORC), University of Southampton, Southampton, U.K., as a Marie Curie Fellow. Since 2012, he has been with Shenzhen University, Shenzhen, China, as a Distinguished Professor. He has authored or co-authored one book, 53 invention patents, and more than 420 journal articles and conference papers. His current research interests focus on optical fiber sensors, fiber gratings, and photonic crystal fibers.

Prof. Wang is a Fellow of Optica and the Chinese Optical Society.

Jun He (Member, IEEE) was born in Hubei, China, in 1985. He received the B.Eng. degree in electronic science and technology from Wuhan University, Wuhan, China, in 2006, and the Ph.D. degree in electrical engineering from the Institute of Semiconductors, Chinese Academy of Sciences (CAS), Beijing, China, in 2011.

From 2011 to 2013, he was with Huawei Technologies, Shenzhen, China, as a Research Engineer. From 2013 to 2015, he was with Shenzhen University, Shenzhen, as a Postdoctoral Research Fellow. From 2015 to 2016, he was with The University of New South Wales (UNSW), Sydney, NSW, Australia, as a Visiting Fellow. Since 2017, he has been with Shenzhen University, as an Assistant Professor/an Associate Professor/a Distinguished Professor. He has authored or co-authored ten invention patents and more than 100 journal articles and conference papers. His current research interests focus on optical fiber sensors, fiber Bragg gratings (FBGs), and fiber lasers.

Prof. He is a member of the Optical Society of America.